J Eng Math (2015) 92:147–165
DOI 10.1007/s10665-014-9769-3

A parametric study of lycopodium dust flame

Mehdi Bidabadi · Hossein Beidaghy Dizaji · Farzad Faraji Dizaji · Seyed Alireza Mostafavi

Received: 29 December 2013 / Accepted: 7 December 2014 / Published online: 24 March 2015

Abstract Dust flames are associated with two-phase combustion phenomena where flame characteristics depend on interactions between solid and gas phases. Since organic dust particles can be effectively utilized in energy production systems, investigation of this phenomenon is essential. In this study, an analytical model is presented to simulate the combustion process of moist organic dust. The flame structure is divided into three zones: preheat zone, reaction zone, and postflame zone. To determine the effects of moisture content and volatile evaporation, the preheat zone is also divided into four subzones: first heating subzone and drying subzone, second heating subzone, and volatile evaporation subzone. The results obtained from the presented model are in reasonable agreement with experimental data for lycopodium particles. An increase in moisture content causes a reduction in burning velocity owing to moisture evaporation resistance. Consequently, the effects of some important parameters, like volatilization temperature, volatilization Damköhler number and drying Damköhler number are investigated. In special cases, like high moisture content, low volatilization temperature, and high drying resistance, the second heating subzone is omitted.

Keywords Burning velocity · Damköhler number · Flame temperature · Micro size particle · Volatilization

1 Introduction

Increasing energy demands and the depletion of fossil fuels have caused humans to explore new resources to satisfy their energy needs. In addition, effective conversion systems have an essential role to play in the future

M. Bidabadi
School of Mechanical Engineering Department of Energy Conversion, Combustion Research Laboratory, Iran University of Science and Technology, Narmak, 16887 Tehran, Iran

H. Beidaghy Dizaji
School of Mechanical Engineering, Department of Aerospace Engineering, Iran University of Science and Technology, 16887 Tehran, Iran

F. Faraji Dizaji
School of Engineering, The University of Vermont, 33 Colchecter Avenue, Burlington, VT 05405, USA

S. A. Mostafavi (✉)
Department of Mechanical Engineering, Faculty of Engineering, Arak University, 38156-88349 Arak, Iran
e-mail: a-mostafavi@araku.ac.ir

of energy production [1–4]. Biomass has been identified as a major renewable resource [5]. Furthermore, power generation from biomass is a CO_2-neutral method and will help us to preserve our environment for future generations. Biomass is presently estimated to contribute on the order of 10–14% of the world's energy supply [6].

Because they have a low energy density, it is not economical to transport biomass fuels to power plants. However, a small-scale biomass conversion system is suitable for local usage. The Stirling engine is one of the best available technologies for small-scale biomass power production; it can be driven by many kinds of heat sources and can be incorporated into biomass energy utilization research projects as a viable prime mover [7–9]. Stirling engines are fed up to 500 μm microscale biomass to enhance their efficiency.

Besides power generation issues, microscale organic dusts demonstrate an extraordinary combustive behavior. Dust explosion occurs in most organic and inorganic dusts. A dust explosion is initiated by the rapid combustion of flammable particulates suspended in the air. Any solid material that can burn in the air will have the same behavior, with a violence and speed that increase with the degree of subdivision of the material. Any solid material have been recognized as a threat to humans and their property for the last 150 years [10].

Generally, combustible particles ignite in two phases: a gaseous and a solid phase. Since most organic particles combust in a gaseous phase, the volatilization and combustion mechanisms of volatile particles needs to be investigated. So far, little research has been done in this area. For example, fundamental information, such as the structure and movement of a combustion zone in a dust particle cloud in a vertical duct, is still ambiguous [11,12]. In general, solid particles heat up until they reach the evaporation temperature; then volatiles come out of the particles, and finally these volatiles combust in a reaction zone.

Unlike dust combustion, flame propagation in a uniformly dispersed spray has been widely studied [13–15]. It has been shown for combustion in liquid sprays that if the overall equivalence ratio of the initial combustible mixture is greater than 0.7, the flame standoff distance is greater than the characteristic separation distance between the liquid droplets [11,16]. This assumption guarantees continuity conditions in the flame structure. This finding regarding spray combustion can be generalized for the combustion of organic dust particles. With respect to organic dust, it is accepted that for small n_s (local number density of particles) in the reaction zone, fuel particles burn with an envelope diffusion flame surrounding each particle. In the present paper, it is assumed that the value of n_s is large enough that the standoff distance of the envelope flame surrounding each particle is much larger than the characteristic separation distance between particles [16]. According to the preceding discussion, our analytical model is valid for $\varphi_u > 0.7$.

In experiments, to measure the explosivity of other types of dust particles and to calibrate dust explosion testing, lycopodium has been used as a reference dust since it has good dispersability and flowability (ISO 1985) [10]. Researchers have conducted many studies on organic dust combustion both experimentally [10,17,18] and analytically [16,19,20].

Laminar flames of lycopodium in air in a dust concentration range of 125–190 g/m^3 has been investigated [21]. Based on the wall cooling effects in these experiments, the maximum achieved burning velocities is similar to those found by Kaesche-Krischer and Zehr [22]. The burning velocity was found to be approximately 0.25 m/s in both experiments.

The effect of gravity on lycopodium dust combustion has been investigated [23]. In the presence of gravity, dust burning velocity was higher compared to free-gravity conditions in an upward stream.

A thermal gravity analysis (TGA) test was used by Han et al. [10] to determine the combustive properties of lycopodium particles. They calculated the burning velocity, flame temperature, and flame length. In their observations, they found that a propagating lycopodium flame front is discontinuous and not smooth. The flame in the spatial area between independent flames or individual burning particles is not observed. The researchers reported that a lycopodium flame cannot move (propagate) continuously in comparison with premixed gaseous flames.

Proust [17] has reported the burning velocity and flame temperature for three different particles; lycopodium, starch, and sulfur. Proust reported that there appeared to be a significant discrepancy between the theoretical and experimental values of maximum flame temperatures. He thought that this difference was a consequence of severe heat losses, but in reality, the mixing with air of combustible vapors produced during the pyrolysis of the particles

Table 1 Brief overview of studies on lycopodium particle cloud combustion

No.	Authors and year	Ref.	Method	Conc. (g/m^3)	V_u (cm/s)
1	Kaesche-Krischer and Zehr (1958), cited by Eckhoff (1997)	[30]	Cylindrical tube $d = 20$ mm	206–509	16–26
2	Kaesche-Krischer (1959), cited by Silvestrini et al. (2008)	[31]	Burner	180–500	25
3	Kaesche-Krischer (1959), cited by Eckhoff (1997)	[30]	–	281–440	33–35
4	Mason and Wilson (1967)	[21]	Cylindrical tube $d = 10.9$ mm (The maximum value of V_u)	193–234	13–25
5	Mason and Wilson (1967)	[21]	Cylindrical tube $d = 10.9$ mm (The average value of V_u)	193–234	11–18
6	Berlad and Killory (1979)	[23]	Freely propagating upward, gravity = 1	130	17
7	Berlad and Killory (1979)	[23]	Freely propagating upward, gravity = 0	130	11
8	Proust and Veyssiere (1988), cited by Silvestrini et al. (2008)	[31]	Square duct $200 \times 200\,\text{mm}^2$	35–100	47
9	Van der Wel (1993), cited by Silvestrini et al. (2008)	[31]	Burner	150–450	30
10	Van der Wel (1993), cited by Silvestrini et al. (2008)	[31]	20-1 sphere	1,000	17
11	Gieras et al. (1995), cited by Silvestrini et al. (2008)	[31]	Square duct $80 \times 80\,\text{mm}^2$	30–230	47
12	Pedersen and van Wingerden (1995), cited by Silvestrini et al. (2008)	[31]	Cylindrical tube $d = 128$ mm	50–175	41
13	Glinka et al. (1996), cited by Silvestrini et al. (2008)	[31]	Cylindrical tube $d = 160$ mm	35–200	69
14	Krause et al. (1996), cited by Silvestrini et al. (2008)	[31]	Cylindrical tube $d = 60$ mm	160–710	28
15	Karause et al. (1996), cited by Silvestrini et al. (2008)	[31]	Cylindrical tube $d = 100$ mm	180–635	50
16	Krause and Kasch (2000), cited by Dyduch and Majcher-Morawiec (2007)	[32]	Cylindrical tube $d = 300$ mm	125–637	25–51
17	Krause and Kasch (2000)	[33]	Cylindrical tube $d = 300$ mm	125–635	15–40
18	Han et al. (2000)	[10]	Square duct $150 \times 150\,\text{mm}^2$	46–590	37–51
19	Proust (2006)	[17]	Square duct $100 \times 100\,\text{mm}^2$, tube method (correlation)	37–92	25–45
20	Proust (2006)	[17]	Square duct $100 \times 100\,\text{mm}^2$, tube method	45–92	25–48
21	Proust (2006)	[17]	Square duct $100 \times 100\,\text{mm}^2$, direct method	37–65.03	9–33
22	Dyduch and Majcher-Morawiec (2007)	[32]	Analytical model	150–1,500	34–66
23	Van Wingerden et al. (2009)	[18]	Cylindrical tube $d = 128$ mm	50–100	25–30
24	Han (2009)	[34]	Square duct $150 \times 150\,\text{mm}^2$	46–590	34–43

Table 1 continued

No.	Authors and year	Ref.	Method	Conc. (g/m^3)	V_u (cm/s)
25	Han et al. (2009)	[35]	Analytical model	46–600	17–19
26	Bidabadi and Rahbari (2009)	[19]	Analytical model	35–95	9–14
27	Bidabadi et al. (2010)	[25]	Analytical model	10–100	12–41
28	Bidabadi et al. (2013)	[20]	Analytical model	35–95	14–21
29	Bidabadi et al. (2014)	[24]	Analytical model	35–95	22–35
30	Present work	–	Analytical model	20–190	15–33

could not proceed to completion at the onset of combustion; consequently, the oxidation in the reaction zone of the flame was not complete.

Seshadri et al. [16] studied analytically the structure of premixed flames propagating in combustible systems containing uniformly distributed volatile fuel particles in an oxidizing gas mixture. Bidabadi et al. [19] presented an analytical model for lycopodium dust combustion considering the temperature difference between gas and particles. Bidabadi et al. [24] calculated the effect of radiation emitted from the preheat reaction zone to the preheat zone and reported that taking into consideration the radiation mechanism has improved the burning velocity. A brief overview of previous researches carried out on lycopodium dust combustion fields is presented in Table 1.

In the present study, the flame propagation mechanism and the structure of the combustion zone are analytically investigated in order to clarify the mechanisms of flame propagation through moist dust clouds. The moisture content changes the flame structure, burning velocity, and flame temperature. Our last model [25] was developed to investigate the effect of moisture content. Also in this article, the effects of the Damköhler numbers (Da_{vap} and Da_{dry}) on the combustion phenomena of organic dust particles are studied. In fact, the Damköhler numbers (Da_{vap} and Da_{dry}) represent the tendency of particles to evaporate. These parameters have a large effect on the combustive behavior of organic particles. For example, particles that tend to evaporate in a highly volatile way combust quickly. In the present model, it is presumed that the moisture content of the solid particles evaporates first, then the dried particles vaporize to yield a gaseous fuel (CH_4); finally, the produced gaseous fuel combusts in a thin reaction zone. In the next section, all of the required equations are introduced and then solved using some assumptions and simplifications. In the results section, some of the effective parameters on flame propagation are explained. Then the conditions in which the second heating subzone can be omitted and in which the presented model eventually turns into a three-subzone model is investigated.

2 Theoretical model

The Lewis number (Le) for organic dust materials is defined as follows:

$$\mathrm{Le} = \frac{\lambda}{\rho C D}, \tag{1}$$

where λ, ρ, C, and D are the thermal conductivity of the gaseous mixture, mixture density, mixture-specific heat, and characteristic mass diffusivity, respectively. In this study, the Lewis number is assumed to be unity [16,25].

In this article, it is assumed that a reaction occurs in a thin zone $O(1/\mathrm{Ze})$, whereas preheat and postflame zones are quite large. This assumption is based on a high Zeldovich number, which is defined as follows:

$$\mathrm{Ze} = \frac{E(T_f - T_u)}{RT_f^2}, \tag{2}$$

where E, R, T_f, and T_u are the activation energy of the reaction, the universal gas constant, the flame temperature, and the fresh mixture temperature, respectively.

The Damköhler number has various definitions [26,27]. While it is traditionally defined as the ratio of characteristic fluid mechanical time to characteristic chemical time, the volatilization Damköhler number ($\mathrm{Da_{vap}}$) used in this study is defined as the ratio of volatilization time (τ_{vap}) to characteristic reaction time (τ_{chem}) or the ratio of chemical reaction rate to volatilization rate:

$$\mathrm{Da_{vap}} = \frac{\tau_{\mathrm{vap}}}{\tau_{\mathrm{chem}}}. \tag{3}$$

Another dimensionless number that appears in this study is the drying Damköhler number ($\mathrm{Da_{dry}}$), which takes into account the effect of the moisture content. Moisture exists in biomass either as bound water, which is held chemically within the cell walls, or as free water, which is stored in the cell cavities. In the drying process, freshly cut or green biomass starts to dry, and initially, the free water evaporates. The fiber saturation point is reached when all the free water is gone, leaving only the bound water within the cell walls [28]. The volatilization resistance of water within biomass particles, which is calculated according to both free and bound water contents, is represented here as

$$\mathrm{Da_{dry}} = \frac{\tau_{\mathrm{dry}}}{\tau_{\mathrm{chem}}}. \tag{4}$$

A one-step overall reaction is used as a combustion process model: $\nu_{\mathrm{F}}[\mathrm{F}] + \nu_{\mathrm{O_2}}[\mathrm{O_2}] \rightarrow \nu_{\mathrm{P}}[\mathrm{P}]$, where the symbols F, $\mathrm{O_2}$, and P denote the fuel, oxygen, and product, respectively, and the quantities ν_{F}, $\nu_{\mathrm{O_2}}$, and ν_{P} denote their stoichiometric coefficients. The governing equations are introduced as follows.

- Solid fuel particle conservation:

$$\rho V \frac{\mathrm{d}Y_{\mathrm{s}}}{\mathrm{d}x} = -\rho_{\mathrm{u}} w_{\mathrm{dry}} - \rho_{\mathrm{u}} w_{\mathrm{vap}}. \tag{5}$$

  In the preceding equation, Y_{s}, V, and ρ denote the mass fraction of organic dust particles, the burning velocity, and the density of the mixture, respectively. $\rho_{\mathrm{u}} = 1.135 \times 10^{-3}\,\mathrm{g/cm^3}$ which is extracted from Seshadri et al. [16]. w_{dry} and w_{vap} are the particle drying rate and volatilization rate, which are expressed by

$$w_{\mathrm{dry}} = \frac{Y_{\mathrm{s}}}{\tau_{\mathrm{dry}}} H\left(T - T_{\mathrm{dry}}\right), \tag{6}$$

$$w_{\mathrm{vap}} = \frac{Y_s}{\tau_{\mathrm{vap}}} H\left(T - T_{\mathrm{vap}}\right), \tag{7}$$

  where H, τ_{dry}, τ_{vap}, T, T_{dry}, and T_{vap} are the Heaviside function, constant characteristic time of drying and volatilization, mixture temperature, and threshold temperature of drying and volatilization, respectively.
- Gaseous fuel conservation:

$$\rho V \frac{\mathrm{d}Y_{\mathrm{g}}}{\mathrm{d}x} = \rho_{\mathrm{u}} D_{\mathrm{u}} \frac{\mathrm{d}^2 Y_{\mathrm{g}}}{\mathrm{d}x^2} - \rho_{\mathrm{u}} w_{\mathrm{chem}} + \rho_u w_{\mathrm{vap}}, \tag{8}$$

  where Y_{g} and D_{u} are respectively the mass fraction of gaseous fuel gained from the volatilization of organic dust particles and the binary diffusion coefficient of the gaseous limiting component. w_{chem} is the rate of chemical-kinetic for lycopodium particles which is defines as below:

$$w_{\mathrm{chem}} = \rho Y_g k, \quad k = B \exp\left(-\frac{E}{RT}\right). \tag{9}$$

  In the preceding equation, B is the frequency factor. $B = 3.5 \times 10^6\,[\mathrm{mol^{-1}s^{-1}}]$, and $E = 96.2\,[\mathrm{kJ/mol}]$ which is extracted from Seshadri et al. [16].
- Energy conservation:

$$\rho V C \frac{\mathrm{d}T}{\mathrm{d}x} = \lambda_{\mathrm{u}} \frac{\mathrm{d}^2 T}{\mathrm{d}x^2} + \rho_{\mathrm{u}} Q w_{\mathrm{chem}} - \rho_{\mathrm{u}} Q_{\mathrm{dry}} w_{\mathrm{dry}} - \rho_{\mathrm{u}} Q_{\mathrm{vap}} w_{\mathrm{vap}}, \tag{10}$$

  where Q_{dry}, Q_{vap}, and Q are the drying heat, volatilization heat, and reaction heat per unit mass of consumed fuel particles, respectively. $Q = 50{,}009\,\mathrm{kJ/kg}$ fuel, $Q_{\mathrm{vap}} = 500.09\,\mathrm{kJ/kg}$ water, and $\lambda_{\mathrm{u}} = 1.46 \times 10^{-3}\,\mathrm{J/(cm\,s\,K)}$ which is extracted from Seshadri et al. [16]. $Q_{\mathrm{dry}} = 2{,}257\,\mathrm{kJ/kg}$ water was taken from thermodynamic tables.

C is the heat capacity of a mixture:

$$C = C_{\mathrm{p}} + \frac{4\pi r_{\mathrm{p}}^3 C_{\mathrm{s}} \rho_{\mathrm{s}} n_{\mathrm{s}}}{3\rho}, \tag{11}$$

where ρ_{s}, r_{p}, n_{s}, (C_{p}), and (C_{s}) are the particle density, particle radius, average number of particles per unit volume, heat capacity of the gas, and heat capacity of the mixture, respectively. $\rho_s = 1\,\mathrm{g/cm^3}$ which is extracted from Seshadri et al. [16].

3 Nondimensionalization of governing equations

Dimensionless parameters are defined as follows:

$$\theta = \frac{T - T_{\mathrm{u}}}{T_{\mathrm{f}} - T_{\mathrm{u}}}, \quad Z = \frac{\rho_{\mathrm{u}} V_{\mathrm{u}} C}{\lambda_u} x, \quad \tau_{\mathrm{chem}} = \frac{\lambda_{\mathrm{u}}}{\rho_{\mathrm{u}} V_{\mathrm{u}}^2 C}, \quad y_{\mathrm{g}} = \frac{Y_{\mathrm{g}}}{Y_{\mathrm{FC}}}, \quad y_{\mathrm{s}} = \frac{Y_{\mathrm{s}}}{Y_{\mathrm{FC}}}, \quad m = \frac{\rho V}{\rho_{\mathrm{u}} V_{\mathrm{u}}}. \tag{12}$$

In the preceding equations, $\theta = 0$ states the dimensionless unburned mixture temperature and $\theta = 1$ the dimensionless flame temperature. In addition, T_{f} and V_{u} are respectively the flame temperature and burning velocity. Y_{FC} is defined as

$$Y_{\mathrm{FC}} Q = C(T_{\mathrm{f}} - T_{\mathrm{u}}). \tag{13}$$

Consequently, the dimensionless governing equations (5), (8), and (10) are obtained as follows:

$$m \frac{\mathrm{d}y_{\mathrm{s}}}{\mathrm{d}Z} = -\frac{y_{\mathrm{s}}}{\mathrm{Da}_{\mathrm{dry}}} H\big(\theta - \theta_{\mathrm{dry}}\big) - \frac{y_{\mathrm{s}}}{\mathrm{Da}_{\mathrm{vap}}} H\big(\theta - \theta_{\mathrm{vap}}\big), \tag{14}$$

$$m \frac{\mathrm{d}y_{\mathrm{g}}}{\mathrm{d}Z} = \frac{1}{\mathrm{Le}} \frac{\mathrm{d}^2 y_{\mathrm{g}}}{\mathrm{d}Z^2} + \frac{y_{\mathrm{s}}}{\mathrm{Da}_{\mathrm{vap}}} H\big(\theta - \theta_{\mathrm{vap}}\big) - \hat{\dot{w}}_{\mathrm{chem}}, \tag{15}$$

$$m \frac{\mathrm{d}\theta}{\mathrm{d}Z} = \frac{\mathrm{d}^2\theta}{\mathrm{d}Z^2} - \frac{q_{\mathrm{dry}}}{\mathrm{Da}_{\mathrm{dry}}} y_{\mathrm{s}} H\big(\theta - \theta_{\mathrm{dry}}\big) - \frac{q_{\mathrm{vap}}}{\mathrm{Da}_{\mathrm{vap}}} y_{\mathrm{s}} H\big(\theta - \theta_{\mathrm{vap}}\big) + \hat{\dot{w}}_{\mathrm{chem}}. \tag{16}$$

The definitions of q_{vap} and q_{dry} are as follows:

$$q_{\mathrm{vap}} = \frac{Q_{\mathrm{vap}}}{Q}, \quad q_{\mathrm{dry}} = \frac{Q_{\mathrm{dry}}}{Q}. \tag{17}$$

Volatilization Damköhler $\mathrm{Da}_{\mathrm{vap}}$ and drying Damköhler $\mathrm{Da}_{\mathrm{dry}}$ numbers and $\hat{\dot{w}}_{\mathrm{chem}}$ are expressed as follows:

$$\mathrm{Da}_{\mathrm{dry}} = \frac{\tau_{\mathrm{dry}}}{\tau_{\mathrm{chem}}}, \quad \mathrm{Da}_{\mathrm{vap}} = \frac{\tau_{\mathrm{vap}}}{\tau_{\mathrm{chem}}}, \tag{18}$$

$$\hat{\dot{w}}_{\mathrm{chem}} = D_{\mathrm{th}} \frac{k Y_{\mathrm{g}}}{V_{\mathrm{u}}^2} \exp\left(-\frac{\mathrm{Ze}(1-\theta)}{1-\beta(1-\theta)}\right). \tag{19}$$

Also, θ_{dry}, θ_{vap}, and β are described as

$$\theta_{\mathrm{dry}} = \frac{T_{\mathrm{dry}} - T_{\mathrm{u}}}{T_{\mathrm{f}} - T_{\mathrm{u}}}, \quad \theta_{\mathrm{vap}} = \frac{T_{\mathrm{vap}} - T_{\mathrm{u}}}{T_{\mathrm{f}} - T_{\mathrm{u}}}, \quad \beta = \frac{T_{\mathrm{f}} - T_{\mathrm{u}}}{T_{\mathrm{f}}}, \quad D_{\mathrm{th}} = \frac{\lambda_{\mathrm{u}}}{\rho C}. \tag{20}$$

4 Flame structure and evaluation of flame characteristics

To partition the flame structure and solve the governing equations, we should neglect some insignificant terms and use some simplifications in each zone. When Ze tends to positive infinity ($\mathrm{Ze} \to +\infty$), the reaction rate is negligible everywhere except in a small zone located near $Z = 0$, where $\theta = 1$.

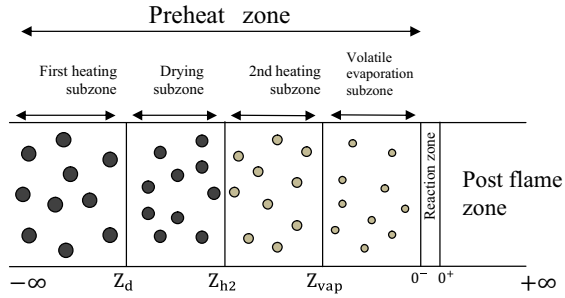

Fig. 1 Schematic figure of combustion regions for presented model

Based on the preceding discussion, the flame structure is divided into three regions:

$$\begin{aligned}
&\text{preheat zone:} && Z_1 = \left\{ Z \,|\, -\infty < Z < 0^- \right\},\\
&\text{asymptotically thin reaction zone:} && Z_2 = \left\{ Z \,|\, 0^- < Z < 0^+ \right\},\\
&\text{post-flame zone:} && Z_3 = \left\{ Z \,|\, 0^+ < Z < +\infty \right\}.
\end{aligned} \tag{21}$$

The preheat zone is a very important in analysis of flame structure, thus this zone itself is divided into four subzones for a better understanding [29]. These subzones are explained below.

$$Z = Z_1 \rightarrow \begin{cases}
\text{first heating subzone:} & Z_{1a} = \{ Z \,|\, -\infty < Z < Z_d \},\\
\text{drying subzone:} & Z_{1b} = \{ Z \,|\, Z_d < Z < Z_{h2} \},\\
\text{second heating subzone:} & Z_{1c} = \left\{ Z \,|\, Z_{h2} < Z < Z_{vap} \right\},\\
\text{volatile evaporation subzone:} & Z_{1d} = \left\{ Z \,|\, Z_{vap} < Z < 0^- \right\}.
\end{cases} \tag{22}$$

The first heating subzone is a region where particles heat up to $T = T_{dry}$, and there is no change in weight of the particles. In the drying subzone, particles' moisture evaporates in a temperature-increasing process and water vapor is produced. This water vapor diffuses to the previous and the next subzones. In the second heating subzone, the temperature of the particles increases up to volatilization temperature. Finally, in the volatile evaporation subzone, the particles vaporize to yield a gaseous fuel. The gaseous fuel also diffuses to other regions. Because of diffusion phenomena, there is no sharp change in the temperature and quantities of the gaseous fuel. The flame structure of organic dust particles is shown in Fig. 1.

To obtain the flame structure, an analytical method is used to solve the governing equations with existing boundary conditions and a matching condition.

(1) The required boundary conditions for the subzone I are as follows:

$$\text{at} \quad Z \rightarrow -\infty \quad \Rightarrow \quad y_s = \alpha, \quad y_g = 0, \quad \theta = 0. \tag{23}$$

At the border of the first heating and drying subzones, the boundary conditions are as follows:

$$\begin{aligned}
&\text{at} \quad Z = Z_d \quad \Rightarrow \quad \theta = \theta_d, \quad y_s = \alpha,\\
&Z = Z_d \rightarrow \begin{cases}
y_s|_{Z_d^-} = y_s|_{Z_d^+},\\
y_g|_{Z_d^-} = y_g|_{Z_d^+},\\
\frac{dy_g}{dZ}|_{Z_d^-} = \frac{dy_g}{dZ}|_{Z_d^+}.
\end{cases}
\end{aligned} \tag{24}$$

Equation (24) demonstrates the continuity in the domain, which means there is no change in the quantity of mass fraction of solid and gaseous fuel at the borders. In addition, the diffusivity of gaseous fuel causes no change in the derivative of gaseous fuel (mass fraction) concentration.

At the interface of the drying and the second heating subzones, the boundary conditions are as follows:

$$\text{at} \quad Z = Z_{h2} \quad \Rightarrow \quad \theta = \theta_{h2}, \quad y_s = \alpha',$$

$$Z = Z_{h2} \rightarrow \begin{cases} y_{\mathrm{s}}|_{Z_{h2}^-} = y_{\mathrm{s}}|_{Z_{h2}^+}, \\ y_{\mathrm{g}}|_{Z_{h2}^-} = y_{\mathrm{g}}|_{Z_{h2}^+}, \\ \frac{\mathrm{d}y_{\mathrm{g}}}{\mathrm{d}Z}\big|_{Z_{h2}^-} = \frac{\mathrm{d}y_{\mathrm{g}}}{\mathrm{d}Z}\big|_{Z_{h2}^+}. \end{cases} \tag{25}$$

Finally, at the interface of the second heating and the volatile evaporation subzones, the boundary conditions are as follows:

$$\text{at} \quad Z = Z_{\mathrm{vap}} \quad \Rightarrow \quad \theta = \theta_{\mathrm{vap}}, \quad y_s = \alpha',$$

$$Z = Z_{\mathrm{vap}} \rightarrow \begin{cases} y_{\mathrm{s}}|_{Z_{\mathrm{vap}}^-} = y_{\mathrm{s}}|_{Z_{\mathrm{vap}}^+}, \\ y_{\mathrm{g}}|_{Z_{\mathrm{vap}}^-} = y_{\mathrm{g}}|_{Z_{\mathrm{vap}}^+}, \\ \frac{\mathrm{d}y_{\mathrm{g}}}{\mathrm{d}Z}\big|_{Z_{\mathrm{vap}}^-} = \frac{\mathrm{d}y_{\mathrm{g}}}{\mathrm{d}Z}\big|_{Z_{\mathrm{vap}}^+}. \end{cases} \tag{26}$$

(2) At the interface of the volatile evaporation subzone and the reaction zone, the boundary conditions are as follows:

$$\text{at} \quad Z \rightarrow 0^- \quad \Rightarrow \quad \theta = 1, \quad y_{\mathrm{g}} = 0. \tag{27}$$

(3) Convection and volatilization terms are considered to be negligible in the reaction zone in comparison with reaction and diffusion terms. The integration of reactive diffusive equations (15) and (16) in the reaction zone gives the following matching condition:

$$\left[\frac{\mathrm{d}\theta}{\mathrm{d}Z} + \frac{1}{\mathrm{Le}}\frac{\mathrm{d}y_{\mathrm{g}}}{\mathrm{d}Z}\right]_{0^-} = \left[\frac{\mathrm{d}\theta}{\mathrm{d}Z} + \frac{1}{\mathrm{Le}}\frac{\mathrm{d}y_g}{\mathrm{d}Z}\right]_{0^+}. \tag{28}$$

As discussed previously, in the preheat zone the reaction term is neglected in favor of the convection and diffusion terms. q_{vap} is also a negligible quantity (close to zero) in comparison with other terms of the energy conservation equation, which means that heat released from a reaction is greater than heat absorbed by particles for volatilization. Thus, q_{vap} will not be considered in the energy equation. To solve the conservation equations analytically, q_{dry} is also assumed to be negligible. To compensate for the effect of q_{dry}, the moisture evaporation effect should be considered in the solution of the energy equation. Thus, the energy equation and its boundary conditions are written as follows:

$$m\frac{\mathrm{d}\theta}{\mathrm{d}Z} = \frac{\mathrm{d}^2\theta}{\mathrm{d}Z^2} \xrightarrow{\text{assuming } m=1} \frac{\mathrm{d}^2\theta}{\mathrm{d}Z^2} - \frac{\mathrm{d}\theta}{\mathrm{d}Z} = 0, \tag{29}$$

$$\theta = C_1 \exp(Z) + C_2,$$

$$\begin{cases} Z = -\infty \rightarrow \theta = 0 \rightarrow C_2 = 0, \\ Z = 0 \rightarrow \theta = 1 \rightarrow C_1 = 1. \end{cases} \tag{30}$$

The dimensionless temperature is defined as

$$\theta = \exp(Z), \quad Z \leq 0. \tag{31}$$

To consider the effect of moisture content (M), a coefficient $F[M, \phi_{\mathrm{u}}]$ is multiplied by the final solution of the problem where T_{f} appears, and it is defined as follows:

$$F[M, \phi_{\mathrm{u}}] = \frac{T_{\mathrm{b}}[M, \phi_{\mathrm{u}}]}{T_{\mathrm{b}}[M = 0, \phi_{\mathrm{u}}]}. \tag{32}$$

This coefficient is obtained by comparing the adiabatic temperatures of a gaseous fuel (CH_4), which is obtained from thermodynamics, to a gaseous fuel with water content. As shown in Fig. 2, it is clear that increasing the moisture content causes a decrease in the adiabatic flame temperature of the gaseous fuel and $F[M, \phi_{\mathrm{u}}]$.
φ_u is defined in the following equations [16]:

$$\varphi_{\mathrm{u}} = \frac{17.18 Y_{\mathrm{Fu}}}{1 - Y_{\mathrm{Fu}}}, \qquad \varphi_{\mathrm{g}} = \frac{17.18 Y_{\mathrm{FC}}}{1 - Y_{\mathrm{FC}}}. \tag{33}$$

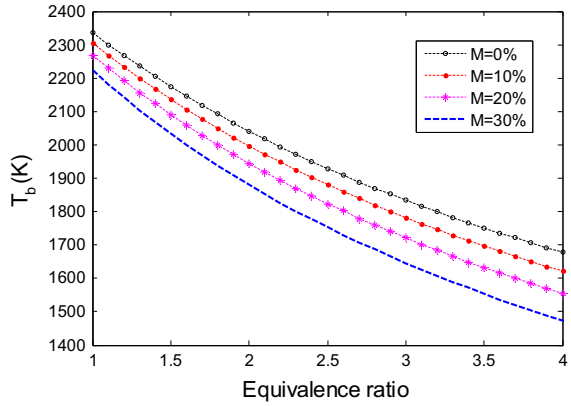

Fig. 2 Variation in adiabatic flame temperature as a function of φ_u (equivalence ratio) for different moisture contents

For wet particles the definition of φ_u and φ_g are written as a function of moisture content (M):

$$\varphi_u = \frac{Y_{Fu}(274.56 + 18M)}{16(1 - Y_{Fu})}, \quad \varphi_g = \frac{Y_{FC}(274.56 + 18M)}{16(1 - Y_{FC})}. \tag{34}$$

In the preceding equations, Y_{Fu} and Y_{FC} are defined as follows:

$$Y_{Fu} = \alpha Y_{FC}, \quad Y_{FC} = \frac{C(T_f - T_u)}{Q}. \tag{35}$$

4.1 First heating subzone ($-\infty < Z < Z_d$)

In this subzone ($-\infty < Z < Z_d$), the particles only heat up to $T = 100\,^{\circ}\mathrm{C}$ and start to dry. Consequently, there is no change in the mass fraction of the particles:

$$y_s = y_s|_{-\infty} = y_s|_{Z_d} = \alpha, \quad \alpha = \frac{Y_s|_{-\infty}}{Y_{FC}}, \tag{36}$$

where Y_{FC} is as defined in Eq. (13). No gaseous fuel is produced in this subzone. To evaluate the mass fraction of the gaseous fuel, the diffusion and convection terms are considered while other terms are assumed to be negligible. Thus:

$$y_g = B_1 \exp(\mathrm{Le}\ Z) + B_2. \tag{37}$$

The boundary conditions force B_2 to be zero, and the quantity of B_1 is obtained by applying the boundary condition between the first heating and the drying subzones. This boundary condition is also coupled with other matching conditions.

4.2 Drying subzone ($Z_d < Z < Z_{h2}$)

In this subzone, moisture evaporation causes the particles to lose their weight. The mass fraction of the particles can be determined using the following equation:

$$\begin{aligned} &\frac{dy_s}{dZ} = -\frac{y_s}{Da_{dry}}, \\ &Z = Z_d \rightarrow y_s = y_s|_{-\infty} = \alpha, \\ &y_s = \alpha \exp\left(\frac{Z_d - Z}{Da_{dry}}\right). \end{aligned} \tag{38}$$

Now this equation is used to calculate Z_{h2}:

$$y_s = \alpha' \quad \Rightarrow \quad Z_{h_2} = -\mathrm{Da}_{\mathrm{dry}} \ln\left(\frac{\alpha'/\alpha}{\exp\left(\frac{Z_\mathrm{d}}{\mathrm{Da}_{\mathrm{dry}}}\right)}\right), \quad \alpha' = \frac{Y_\mathrm{s}|_{Z_{\mathrm{vap}}}}{Y_{\mathrm{FC}}}. \tag{39}$$

Also, Z_d is calculated using Eq. (31) by considering the fact that the drying temperature of the material is known, (T_d).

For gaseous fuel, the mass fraction distribution is the same as in the previous subzone:

$$y_\mathrm{g} = D_1 \exp(\mathrm{Le}\ Z) + D_2. \tag{40}$$

4.3 Second heating subzone ($Z_{h2} < Z < Z_{\mathrm{vap}}$)

This subzone is similar to the first heating subzone; boundary temperatures are the only difference between them. In addition, there is no change in the weight of the particles and no gaseous fuel is produced. However, gaseous fuel diffuses from the next subzone (volatile evaporation subzone). Thus,

$$y_\mathrm{s} = y_\mathrm{s}|_{Z_{h2}} = \alpha', \tag{41}$$

$$y_\mathrm{g} = E_1 \exp(\mathrm{Le}\ Z) + E_2. \tag{42}$$

Z_{vap} is calculated using Eq. (31) and the pyrolysis temperature of the material (T_{vap}).

4.4 Volatile evaporation subzone ($Z_{\mathrm{vap}} < Z < 0^-$)

This subzone is the most important region in the flame structure. In this subzone, gaseous fuel is produced and then diffuses to other regions. The mass fraction of the particles is determined to as

$$\frac{\mathrm{d}y_\mathrm{s}}{\mathrm{d}Z} = -\frac{y_\mathrm{s}}{\mathrm{Da}_{\mathrm{vap}}},$$

$$Z = Z_{\mathrm{vap}} \rightarrow y_s = \alpha', \tag{43}$$

$$y_s = \alpha' \exp\left(\frac{Z_{\mathrm{vap}} - Z}{\mathrm{Da}_{\mathrm{vap}}}\right).$$

The amount of unburned solid mass is calculated using the following expression:

$$Z = 0^- \Rightarrow y_{\mathrm{s(rem)}} = \alpha' \exp\left(\frac{Z_{\mathrm{vap}}}{\mathrm{Da}_{\mathrm{vap}}}\right). \tag{44}$$

Finally, the gaseous fuel in this subzone is evaluated using the following equation:

$$y_g = I_1 \exp(\mathrm{Le}\ Z) + I_2 - \frac{\mathrm{Le}\,\alpha'}{\frac{1}{\mathrm{Da}_{\mathrm{vap}}} + \mathrm{Le}} \exp\left(\frac{Z_{\mathrm{vap}} - Z}{\mathrm{Da}_{\mathrm{vap}}}\right). \tag{45}$$

The constants in the gaseous fuel distribution in all subzones are dependent on each other and can be determined by solving eight equations simultaneously using existing boundary conditions.

4.5 Postflame zone ($0^+ < Z < +\infty$)

Before analyzing the reaction zone, the postflame zone is investigated in depth:

$$\theta = 1, \quad y_\mathrm{s} = \text{constant}, \quad y_\mathrm{g} = 0. \tag{46}$$

In the postflame zone, the available mass fraction of solid particles is approximately equal to the quantity of y_s at the end of the volatilization zone (i.e., $Z = 0^-$).

4.6 Reaction zone ($0^- < Z < 0^+$)

In this region, the convective and volatilization terms, in the conservation equations, are too small in comparison with the diffusive and reactive terms. To analyze the structure of this zone, the following expressions are introduced:

$$\eta = \frac{Z}{\varepsilon}, \quad y^* = \frac{y_g - y_{gF}}{\varepsilon}, \quad t = \frac{1-\theta}{\varepsilon}, \quad \varepsilon = \frac{1}{\mathrm{Ze}}, \tag{47}$$

where η, y^*, and t are expanded using the expansion parameter $\varepsilon = 1/\mathrm{Ze}$. This expansion parameter is presumed to be small. Substituting the expansion relations into the gaseous fuel and energy conservation equations (15) and (16), they yield the following expressions, respectively:

$$\frac{D_{th} k \varepsilon^2}{V_u^2}\left(y^* + b\right)\exp(-t) = \frac{1}{\mathrm{Le}}\frac{\mathrm{d}^2 y^*}{\mathrm{d}\eta^2}, \tag{48}$$

$$\frac{D_{th} k \varepsilon^2}{V_u^2}\left(y^* + b\right)\exp(-t) = \frac{\mathrm{d}^2 t}{\mathrm{d}\eta^2}. \tag{49}$$

In the preceding equations, $b = y_{gF}/\varepsilon$, in which y_{gF} is the amount of gaseous fuel at the beginning of the reaction zone.

Combining Eqs. (48) and (49) and using some mathematical operations, it is possible to obtain the burning velocity, which is the main purpose of this article:

$$V_u^2 = \frac{2\lambda B}{\mathrm{Ze}^2 \rho C}\left[\mathrm{Ze}\left\{I_1 \exp\left(-\frac{\mathrm{Le}}{\mathrm{Ze}}\right) + I_2 + F_1 \exp\left(\frac{1}{\mathrm{Da_{vap}Ze}}\right)\right\} + \mathrm{Le}\right]\exp\left(-\frac{E}{RT_f F[M, \phi_u]}\right). \tag{50}$$

In the preceding equations, ϕ_u is the equivalence ratio based on fuel available in the particles in the ambient reactant stream. Both expressions on the right-hand side of the matching equation are too small (according to Eq. 46) and can be neglected:

$$\left[\frac{\mathrm{d}\theta}{\mathrm{d}Z} + \frac{1}{\mathrm{Le}}\frac{\mathrm{d}y_g}{\mathrm{d}Z}\right]_{0^-} = \left[\frac{\mathrm{d}\theta}{\mathrm{d}Z} + \frac{1}{\mathrm{Le}}\frac{\mathrm{d}y_g}{\mathrm{d}Z}\right]_{0^+}.$$

Now, replacing the left-hand side with correlations leads to a relation between $\mathrm{Da_{vap}}$, Ze, Le, and θ_{vap}:

$$\exp\left(-\frac{1}{\mathrm{Ze}}\right) + I_1 \exp\left(-\frac{\mathrm{Le}}{\mathrm{Ze}}\right) - \frac{F_1}{\mathrm{Da_{vap}\ Le}}\exp\left(\frac{1}{\mathrm{Da_{vap}\ Ze}}\right) = 0, \tag{51}$$

where F_1, I_1, and I_2 are obtained from Eq. (45):

$$\begin{aligned}
F_1 &= \frac{-\mathrm{Le}\alpha' \exp\left(\frac{Z_{vap}}{\mathrm{Da_{vap}}}\right)}{\left(\frac{1}{\mathrm{Da_{vap}}} + \mathrm{Le}\right)},\\
I_1 &= -\left(\frac{-\left(\frac{F_1}{\mathrm{Da_{vap}}}\right)\exp\left(-\frac{Z_{vap}}{\mathrm{Da_{vap}}}\right)}{\mathrm{Le}}\right) + F_1\left(\exp\left(-\frac{Z_{vap}}{\mathrm{Da_{vap}}}\right) - 1\right),\\
I_2 &= \left(\frac{\mathrm{Da_{vap}\ Le}\ \alpha'}{\mathrm{Le\ Da_{vap}} + 1}\right)\left(\frac{1 - \mathrm{Le\ Da_{vap}}}{\mathrm{Le\ Da_{vap}}}\right)\left(\exp\left(\frac{-Z_{vap}}{\mathrm{Da_{vap}}}\right)\right)^2.
\end{aligned} \tag{52}$$

5 Results and discussion

To predict flame characteristics, such as burning velocity and mass fractions of the solid and gas, the implicit expression for the burning velocity in Eq. (50) should be solved simultaneously with Eq. (51). The iterative process starts with a known ϕ_u and a guess of the temperature. The temperature is plugged into Eq. (50), and the burning

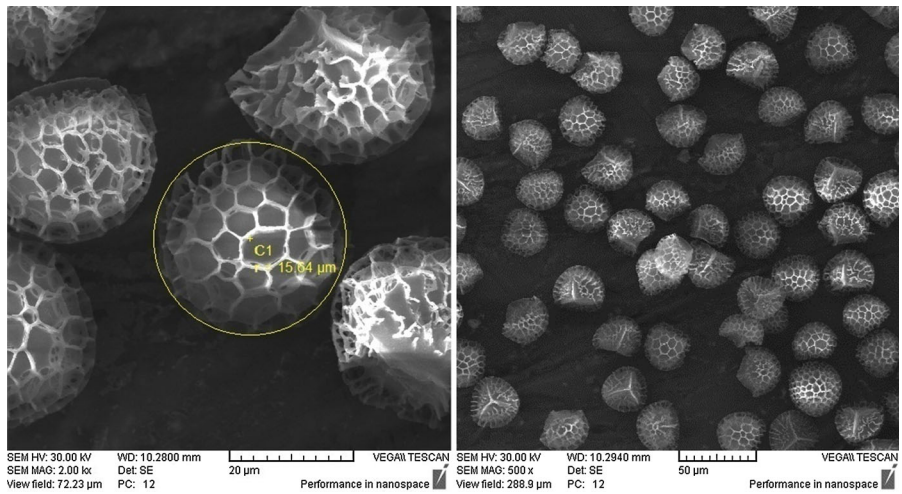

Fig. 3 Picture of lycopodium cluster (SEM laboratory of Iran University of Science and Technology Physics Faculty)

Table 2 A brief overview of works on the radius of lycopodium particles

No.	Authors and year	Ref.	d_p (µm)
1	Han et al. (2000)	[10]	32
2	Han (2009)	[34]	32
3	Han et al. (2009)	[35]	32
4	Berlad and Killory (1979)	[23]	30
5	Proust (2006)	[17]	31
6	Eckhoff (1997)	[30]	30
7	Mason and Wilson (1967)	[21]	30
8	Van Wingerden et al. (1993), cited by Silvestrini et al. (2008)	[31]	32
9	Amyotte and Pegg (1989)	[36]	30
10	Skjold et al. (2013)	[37]	32
11	Bernard et al. (2010)	[38]	31
12	Choi et al. (2001)	[39]	31
13	Beidaghy Dizaji (2011)	[40]	31.3
14	Beidaghy Dizaji et al. (2014)	[41]	31.28
15	Faraji Dizaji (2011)	[42]	31.3
16	Živcova et al. (2007)	[43]	30.6
17	Serzane et al. (2010)	[44]	30
18	Present work	–	31.28

velocity is obtained from this equation. Then both the guessed temperature and the obtained burning velocity are inserted into Eq. (51). If the result is less than 0.001, then both the temperature and the burning velocity are correct. Otherwise, we must make another guess about the temperature and repeat the iterative process. To evaluate the accuracy of the presented model, the burning velocity and the flame temperature are compared with flame velocity and flame temperature using the calculations of previous researchers. Other researchers calculated the burning velocity of lycopodium particles as a function of mass particle concentration using a variety of methods. To compare our results with the experimental data, some initial data (physical characteristics), such as r_p, T_{vap}, Ze, Le, and Da_{vap} of the lycopodium particle, are essential. These parameters are obtained from previous works ($T_{vap} \approx 180\,^{\circ}C$, from a Derivative Thermogravimetry (DTG) analysis of a Thermogravimetry (TG) diagram, which

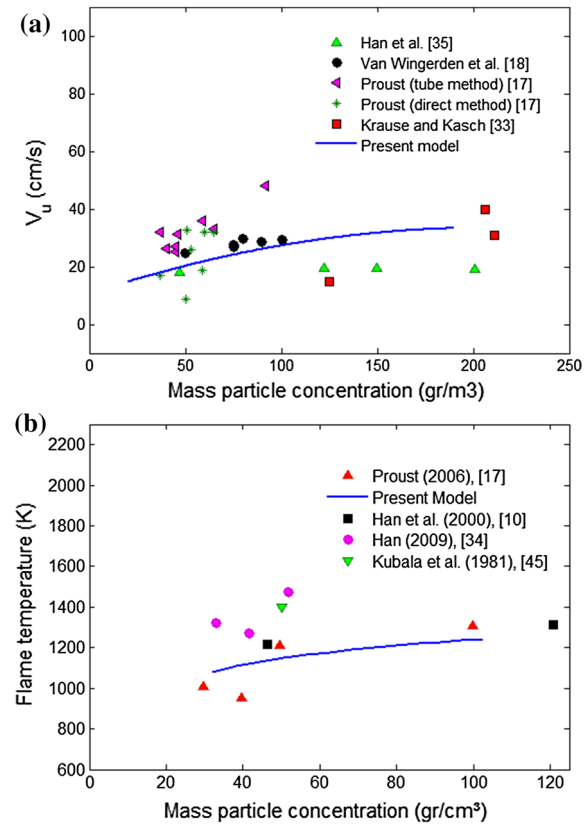

Fig. 4 Variation in burning velocity (**a**) and flame temperature (**b**) as a function of mass particle concentration in the presented model ($Da_{vap} = 0.7$, Le $= 1$, $M = 0\%$, $r_p = 15.5\,\mu m$, $T_{vap} = 453\,K$) and in previous works

Han measured for lycopodium dust particles [10], Ze ≈ 5.5 [16], and Le $= 1$ [16]). As shown in Fig. 3, the radius of a lycopodium particle is approximately $r_p = 15.64\,\mu m$. This measurement is completely compatible with other results (Table 2).

As is shown in Fig. 3, it is reasonable to assume that these particles are mono-size in lycopodium clusters, as reported in Table 2. Using Eq. (51) it is possible to determine Da_{vap}. Since other researchers have calculated the flame velocity and flame temperature for dry lycopodium particles, $F[M, \phi_u] = 1$ is used in Eq. (51). Consequently, Da_{vap} for dry lycopodium particles would be 0.7.

As shown in Fig. 4a, our presented analytical model results for burning velocity as a function of particle concentration are compared with other researchers' experimental results. Also, the flame temperature obtained for the presented model is compared with that of previous works (Fig. 4b). According to Fig. 4, the evolution of the burning velocity and flame temperature as a function of mass particle concentration is in good agreement with experimental data.

There are no experimental data for determining Da_{dry}. However, since the interaction between volatile fuel and the matrix of solid fuel particles is stronger than the interaction between the moisture content and matrix of solid fuel particles, it is possible to assume $Da_{dry} < Da_{vap}$. Based on the physical characteristics of lycopodium, it is assumed that those of other organic dust particles are similar and on the same order as lycopodium dust. As discussed earlier, the overall equivalence ratio of the initial combustible mixture must be larger than 0.7; thus, we present the results for $\varphi_u > 1$ to ensure flame continuity.

According to Fig. 5a, an increase in moisture content causes a reduction in flame temperature. This is due to the latent heat of water. In fact, if the moisture content increases, more heat is consumed to produce the same amount of gaseous fuel. It is worth mentioning that in gas flame analysis, two types of resistance exist against flame propagation: heat transfer resistance and chemical reaction resistance. In dry dust flames, volatilization resistance

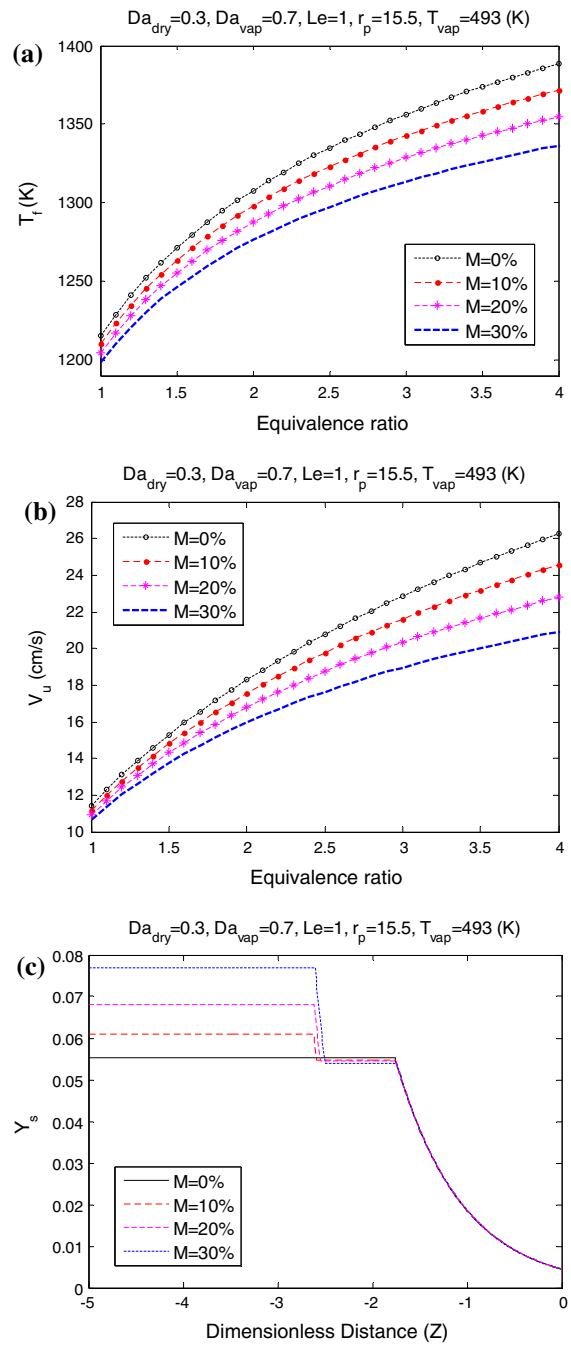

Fig. 5 Variation in flame temperature (**a**), burning velocity (**b**), and organic dust mass fraction (**c**) as a function of dimensionless distance for different moisture contents

is also added to those resistances. In wet dust, moisture evaporation resistance also exists before flame propagation. In fact, the interactions of these resistances in each flame (fuel) control the flame characteristics, like the burning velocity and flame temperature. It is clear that mass transfer resistance exists in all types of the aforementioned flames.

According to Fig. 5b, the burning velocity decreases when the amount of moisture content surges from 0 to 30% at $r_p = 15.5\,\mu m$, $Da_{dry} = 0.3$, $Da_{vap} = 0.7$, and $Le = 1$. As the moisture content in the particle increases, the moisture evaporation resistance also increases. Therefore, flame propagation slows down, which leads to a

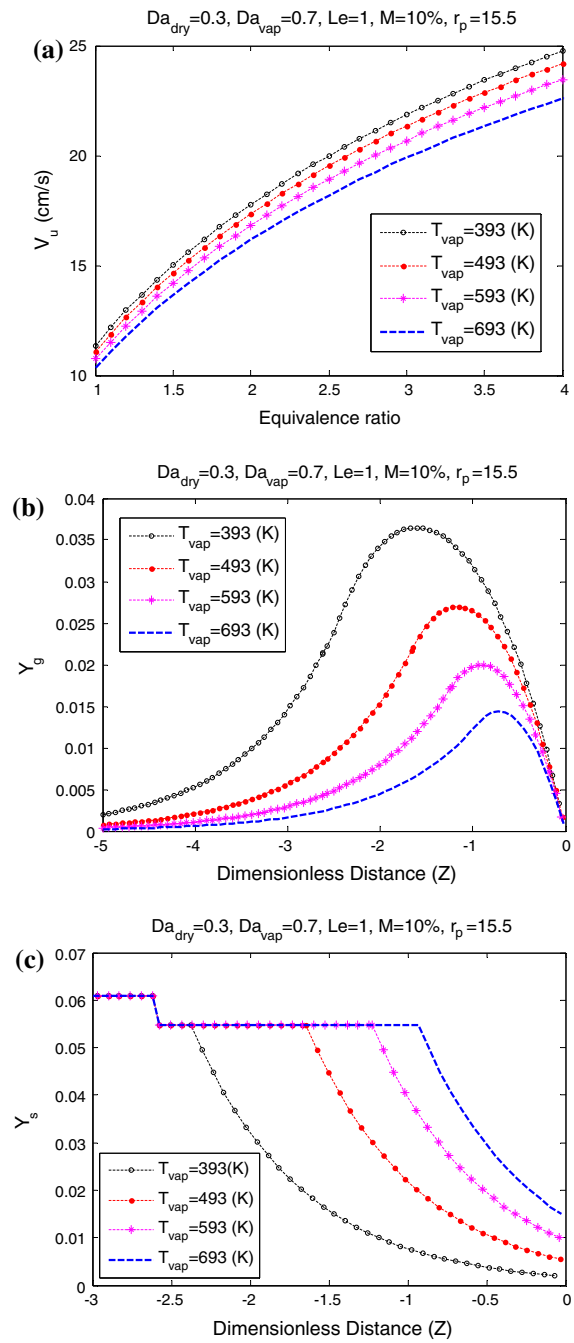

Fig. 6 Variation in burning velocity (**a**), mass fraction of gaseous fuel (**b**), and mass fraction of organic dust (**c**) as a function of dimensionless distance for different volatilization temperatures

decrease in the burning velocity. Also, an increase in the equivalence ratio φ_u (particle number density) reduces the volatilization resistance, and consequently, the burning velocity increases.

As shown in Fig. 5c, it is concluded that an increase in the moisture content causes an increase in the mass fraction of solid particles. This can be illustrated by the following equation:

$$Y_s = \frac{m_{CH_4} + m_{H_2O}}{m_{O_2} + m_{N_2} + m_{CH_4} + m_{H_2O}}.$$

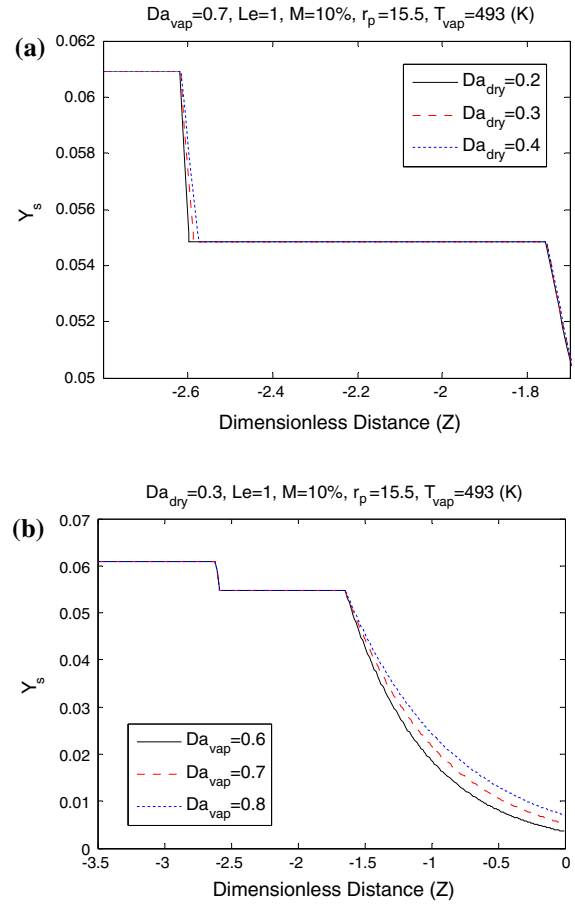

Fig. 7 Variation in mass fraction of solid particles as a function of dimensionless distance for different drying Damköhler numbers Da_{dry} (**a**) and volatilization Damköhler numbers Da_{vap} (**b**)

In the first heating and the drying subzones, the presence of moisture yields a higher mass fraction of solid particles (Y_s). But in the second heating and the volatile evaporation subzones, there is no moisture in the particles. In other words, by omitting H_2O from the numerator of the preceding equation, the denominator of the equation does not change. Thus, for the second heating and the volatile evaporation subzones, the mass fraction (Y_s) of the wetter particles becomes less than that of the drier particles. Since the start points of the drying and volatilization temperatures are considered to be constant, their dimensionless distances from the reference point ($Z = 0$) are almost constant. But the end point of the drying process (which is the start point of the second heating subzone) is greatly affected by the moisture content. By increasing the moisture content, the drying subzone becomes bigger.

Volatilization temperature is one of the essential parameters in the behavior of organic dusts. As shown in Fig. 6a, b, a decrease in the volatilization temperature causes an increase in the burning velocity and mass fraction of the produced gaseous fuel. In fact, if the volatilization temperature decreases, the initiation point of volatilization happens sooner (Fig. 6c).

Clearly any increase in the moisture evaporation resistance (Da_{dry}) will result in a decrease in the burning velocity. Furthermore, it will cause the drying process subzone to become bigger and, consequently, will affect the start point of the second heating zone, as shown in Fig. 7a. An increase in Da_{vap} will also result in a decrease in the rate of volatilization, which means a higher volatilization resistance for a constant reaction rate. Consequently, the burning velocity and mass fraction of the gaseous fuel decrease, and a larger amount of mass fraction (Y_s) is left unburned, as shown in Fig. 7b.

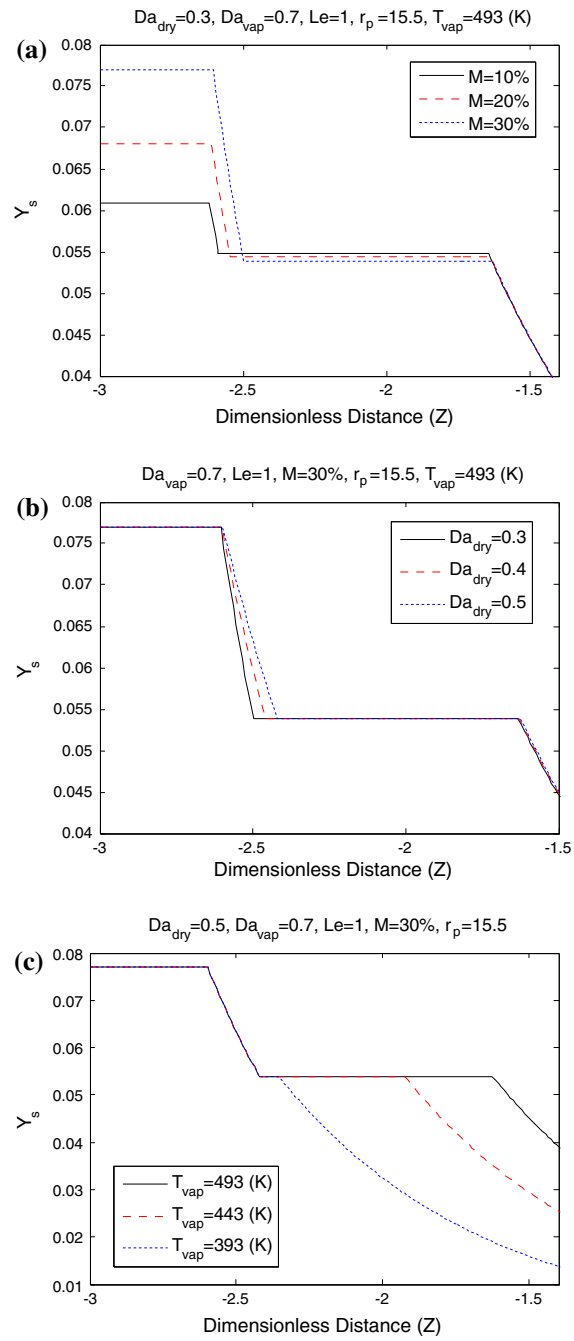

Fig. 8 Effect of different moisture contents (**a**), drying Damköhler numbers (**b**), and devolatilization temperature (**c**) on process of omitting second heating subzone

Finally, the conditions in which the presented model is transformed into a three-subzone model are discussed. From Fig. 8 it is clear that the moisture content, volatilization temperature, and Da_{dry} are effective parameters regarding the structure of the preheat zone. It is also obvious that an increase in the moisture content or Da_{dry} or a decrease in the volatilization temperature will cause the proposed model to transform into a three-subzone model.

6 Conclusion

An analytical model was presented to determine the effects of moisture content on flame characteristics and to investigate the effective parameters for organic dust combustion. To analyze the presented model, it is assumed that, first, the particles vaporize to yield a familiar chemical compound (methane) before starting to combust in the reaction zone. The flame structure is divided into three zones: preheat zone, reaction zone, and postflame zone. The preheat zone is further subdivided into four subzones: the first heating subzone and the drying subzone, the second heating subzone, and the volatile evaporation subzone. This division makes it easier to find the counteraction among various parameters and to view separately the effects of each parameter on the flame structure.

Then the governing equations are nondimensionalized, and these equations with their boundary and matching conditions are simultaneously solved. Consequently, the burning velocity and temperature profiles obtained from this model are compared with previously published experimental data. The comparison demonstrates that the proposed model accurately predicts the behavior of burning velocity and flame temperature.

The results make it clear that an increase in the moisture content causes the flame velocity and flame temperature to decrease. Other physical characteristics of organic particles also affect the flame structure. Volatilization Damköhler number (Da_{vap}) and drying Damköhler number (Da_{dry}) are the determining factors in the combustion of dust particles. It is also seen that an increase in Da_{vap} causes a reduction in the mass fraction of available gaseous fuel and a subsequent decrease in the burning velocity. An increase in the volatilization temperature leads to a decrease in the gaseous fuel mass fraction. In addition, the onset of the volatilization process and the maximum of the diagram move toward the reaction zone.

The present research has shown that an increase in the moisture content or Da_{dry} or a decrease in the volatilization temperature will cause a four-subzone model to switch to a three-subzone model. All the topics discussed in connection with the proposed model are valid for a three-subzone model. However, to avoid repetition, the results of the secondary model are not presented.

References

1. Dincer I (2000) Renewable energy and sustainable development: a crucial review. Renew Sustain Energy Rev 4:157–175
2. Sorensen B (2004) Renewable energy, 3rd edn. Elsevier Science, London
3. Abdullah S, Yousif BF, Sopian K (2005) Design consideration of low temperature differential double acting Stirling engine for solar application. Renew Energy 30:1923–1941
4. Karabulut H, Yucesu HS, Çinar C, Aksoy F (2009) An experimental study on the development of a β-type Stirling engine for low and moderate temperature heat sources. Appl Energy 86:68–73
5. Datta A, Ganguly R, Sarkar L (2000) Energy and exergy analyses of an externally fired gas turbine (EFGT) cycle integrated with biomass gasifier for distributed power generation. Energy 35:341–350
6. Zhao W, Li Z, Zhao G, Zhang F, Zhu Q (1996) Effect of air preheating and fuel moisture on combustion characteristics of corn straw in a fixed bed. Energy Convers Manag 49:3560–3565
7. Carlsen H, Ammundsen N, Traerup J (1996) 40 kW Stirling engine for solid fuel. In: Proceedings of the intersociety energy conversion engineering conference, pp 23–34
8. Jensen N, Werling J (2002) CHP from updraft gasifier and Stirling engine. In: Proceedings of 12th European biomass conference, pp 131–149
9. Lane N, Beale W (1997) Micro-biomass electric power generation. In: Proceedings of the 3rd biomass conference of the Americas, pp 83–104
10. Han OS, Yashima M, Matsuda T, Matsui H, Miyake A, Ogawa T (2000) Behavior of flames propagating through lycopodium dust clouds in a vertical duct. J Loss Prev Process Ind 13:449–457
11. Williams FA (1985) Combustion theory. Addison-Wesley
12. Peters N, Williams FA (1987) The asymptotic structure of stoichiometric methane–air flames. Combust Flame 68:185–207
13. Polymeropoulos CE (1974) Flame propagation in a one-dimensional liquid fuel spray. Combust Sci Technol 9:197–207

14. Ballal DR, Lefebvre AH (1981) Flame propagation in heterogeneous mixtures of fuel droplets, fuel vapor and air. Proc Combust Inst 18:321–328
15. Neophytou A, Mastorakos E (2009) Simulations of laminar flame propagation in droplet mists. Combust Flame 156:1627–1640
16. Seshadri K, Berlad AL, Tangirala V (1992) The structure of premixed particle–cloud flames. Combust Flame 89:333–342
17. Proust C (2006) Flame propagation and combustion in some dust-air mixtures. J Loss Prev Process Ind 19:89–100
18. Van Wingerden K, Stavseng L, Bergen N (2009) Measurements of the laminar burning velocities in dust-air mixtures. http://www.demxs.com/ts-pfiles/file/other/2009-1-4/VDI2.pdf
19. Bidabadi M, Rahbari A (2009) Modeling combustion of *Lycopodium* particles by considering the temperature difference between the gas and the particles. Combust Explos Shock Waves 45:278–285
20. Bidabadi M, Mostafavi SA, Beidaghy Dizaji H, Faraji Dizaji F (2013) Lycopodium dust flame characteristics considering char yield. Scientia Iranica 20(6):1781–1791
21. Mason WE, Wilson MJG (1967) Laminar flames of lycopodium dust an air. Combust Flames 11:195–200
22. Kaesche-Krischer B, Zehr J (1958) Untersuchungen an Staub/Luft-Flammen. Zeitschrift für Physikalische Chemie. New Ser 14:384–387
23. Berlad AI, Killory J (1979) Combustion of porous solids at reduced gravitational conditions. NASA contractor report 3197, State University of New York at Stony Brook, Long Island, New York
24. Bidabadi M, Faraji Dizaji F, Beidaghy Dizaji H, Safari Ghahsareh M (2014) Investigation of effective dimensionless numbers on initiation of instability in combustion of moisty organic dust. J Cent South Univ 21:326–337
25. Bidabadi M, Haghiri A, Rahbari A (2010) The effect of Lewis and Damköhler numbers on the flame propagation through micro-organic dust particles. Int J Therm Sci 49:534–542
26. Liñán A (1981) Lewis number effects on the structure and extinction of diffusion flames due to strain. Lect Notes Phys 136:333–339
27. Vázquez-Espí C, Liñán A (2002) Thermal-diffusive ignition and flame initiation by a local energy source. Combust Theory Model 6:297–315
28. Bryden KM, Hagge MJ (2003) Modeling the combined impact of moisture and char shrinkage on the pyrolysis of a biomass particle. Fuel 82:1633–1644
29. Burgerscentrum JM (2005) Course on Combustion, Chap. 21. Department of Mechanical Engineering, Eindhoven University of Technology
30. Eckhoff RK (1997) Dust explosions in the process industries, 2nd edn. Butterworth Heinemann, Oxford
31. Silvestrini M, Genova B, Leon Trujillo FJ (2008) Correlations for flame speed and explosion overpressure of dust clouds inside industrial enclosures. J Loss Prev Process Ind 21:374–392
32. Dyduch Z, Majcher-Morawiec B (2007) Determination of the laminar burning velocity of dust-air mixtures by applying the model of dust explosion in as closed vessel, Central Mining Institute. Research reports; http://www.gig.eu/files/pdf/2007_2.pdf
33. Krause U, Kasch T (2000) The influence of flow and turbulence on flame propagation through dust-air mixtures. J Loss Prev Process Ind 13:291–298
34. Han OS (2009) Flame propagation characteristics through suspended combustion particles in a full-scaled dust. Korean Chem Eng Res 47:572–579
35. Han OS, Han IS, Choi YR (2009) Prediction of flame propagation velocity based on the behavior of dust particles. Korean Chem Eng Res 47:705–709
36. Amyotte PR, Pegg MJ (1989) Lycopodium dust explosions in a Hartmann bomb: effects of turbulence. J Loss Prev Process Ind 2(2):87–94
37. Skjold T, Olsen KL, Castellanos D (2013) A constant pressure dust explosion experiment. J Loss Prev Process Ind 26:562–570
38. Bernard S, Lebecki K, Gillard P, Youninou L, Baudry G (2010) Statistical method for the determination of the ignition energy of dust cloud-experimental validation. J Loss Prev Process Ind 23:404–411
39. Choi KS, Yamaguma M, Kodama T, Joung JH, Takeuchi M (2001) Characteristics of the vibrating-mesh minimum ignition energy testing apparatus for dust clouds. J Loss Prev Process Ind 14:443–447
40. Beidaghy Dizaji H (2011) Analysis of the effect of dimensionless numbers on organic dust combustion. MSc Thesis, Iran University of Science and Technology (IUST)
41. Beidaghy Dizaji H, Faraji Dizaji F, Bidabadi M (2014) Determining thermo-kinetic constants in order to classify explosivity of foodstuffs. Combust Explos Shock Waves 50(4):452–462
42. Faraji Dizaji F (2011) Analysis of effect of moisture content on combustion of wood dust (Biomass). MSc Thesis, Iran University of Science and Technology (IUST)
43. Živcova Z, Gregorova E, Pabst W (2007) Porous alumina ceramics produced with lycopodium spores as pore-forming agents. J Mater Sci 42:8760–8764
44. Serzane R, Locs J, Berzina-Cimdina L, Sadretdinovs R (2010) Development of porous ceramics by lycopodium using uniaxial pressing and sintering. Process Appl Ceram 4(4):231–235
45. Kubala TA, Perzak FJ, Litchfield EL (1981) Electric ignition of lycopodium powder in a modified Hartmann apparatus. U.S. Department of the Interior, Bureau of Mines, Pittsburgh, PA